J Appl Electrochem (2012) 42:883–891
DOI 10.1007/s10800-012-0464-7

ORIGINAL PAPER

Investigation of lithium ion kinetics through $LiMn_2O_4$ electrode in aqueous Li_2SO_4 electrolyte

Yongli Cui · Zheng Yuan · Wenjing Bao · Quanchao Zhuang · Zhi Sun

Received: 14 May 2012 / Accepted: 22 July 2012 / Published online: 3 August 2012

Abstract Spinel $LiMn_2O_4$ was prepared by sol–gel method and characterized by Fourier transform infrared spectroscopy, X-ray diffraction, and scanning electron microscope. Cyclic voltammogram, galvanostatic charge/discharge testing, and electrochemical impedance spectroscopy (EIS) techniques were employed to evaluate the electrochemical behaviors of $LiMn_2O_4$ in 1 M Li_2SO_4 aqueous solution. Two redox couples at $E_{SCE} = 0.78/0.73$ and 0.91/0.85 V were observed, corresponding to those found at $E_{Li/Li^+} = 4.05/3.95$ and 4.06/4.18 V in organic electrolyte. The discharge capacity of pristine $LiMn_2O_4$ in aqueous electrolyte was 57.57 mAh g^{-1}, and the capacity retention of the electrode is 53.7 % after 60 cycles. Only one semicircle emerged in EIS at different potentials in aqueous electrolyte, while three semicircles were observed in organic electrolytes. There was no solid electrolyte interface film on the surface of spinel $LiMn_2O_4$ electrode in aqueous electrolyte. The change of kinetic parameters of lithium ion insertion in spinel $LiMn_2O_4$ with potential in aqueous electrolyte for initial charge process was discussed in detail, and a suitable model was proposed to explain the impedance response of the insertion materials of lithium ion batteries in different electrolytes.

Keywords Aqueous lithium ion batteries · Spinel $LiMn_2O_4$ · Kinetics · Electrochemical impedance spectroscopy

Y. Cui (✉) · Z. Yuan · W. Bao · Q. Zhuang (✉) · Z. Sun
School of Materials Science and Engineering, China University of Mining and Technology, Xuzhou 221116, China
e-mail: lilyshuoxu@163.com

Q. Zhuang
e-mail: lilyshuoxu@163.com; zhuangquanchao@126.com

1 Introduction

Since commercialization in 1990, lithium ion batteries with intercalation compound electrode and organic electrolyte have been widely used in cameras, laptops, mobile, and other information and communication devices, owing to their advantages of elevated energy density, low self-discharge rate, and long life. Although the performances of nonaqueous lithium ion batteries are often satisfactory, their practical applications are still handicapped by the high cost of strict cell assembly techniques, expensive lithium salts, and severe safety problems arising from the use of highly toxic and flammable solvents, which might cause fires and explosion [1]. Therefore, the application of aqueous lithium ion batteries has recently been seen as an attractive alternative, and increased attention has been paid to their development [2–6], because of inexpensive water soluble salts, the simple cell assembly technology, and environment-friendly characteristics—the ionic conductivity of aqueous electrolytes allowing higher rates and lower voltage drops due to electrolyte's impedance.

For aqueous lithium ion battery, cell potentials must be restricted to the decomposition potential of water. Hence, the selection of intercalation materials which de/intercalate Li ions at an appropriate potential is a key factor for the performance of the aqueous battery due to the evolutions of hydrogen and oxygen from water decomposition [7, 8]. So far, the electrochemical behaviors of the several lithium intercalation compounds in aqueous solution were researched, such as $LiCoO_2$ [7, 9–11], LiV_3O_8 [12–15], TiP_2O_7 [16], $LiTi_2(PO_4)_3$ [16–18], $LiMn_2O_4$ [19, 20], $LiNiPO_4$ [21], TiO_2 [22], and $LiFePO_4$ [23].

However, a detailed knowledge of the lithium ion kinetics through the electrode has not been satisfactorily gleaned in aqueous electrolyte yet, as compared with the

case of organic electrolyte. Lithium manganese oxide ($LiMn_2O_4$) with the cubic spinel structure has been extensively investigated because of its technological application to intercalation electrode. In this article, we focus our attention on the lithium ion kinetics in spinel $LiMn_2O_4$ electrode in 1 M Li_2SO_4 aqueous electrolyte.

2 Experimental

2.1 Preparation of $LiMn_2O_4$ cathode material

$LiMn_2O_4$ was prepared by sol–gel method. Stoichiometric amounts of reactants $C_6H_8O_7{\cdot}H_2O$, $C_4H_6MnO_4{\cdot}4H_2O$, and Li_2CO_3 were dissolved in distilled water to form a mixed aqueous solution. Then, the solutions were added dropwise to a 6 $\sim$ 7 pH of with ammonium hydroxide. The resultant solutions were continuously stirred at 80 °C until a transparent gel was obtained. Later, the prepared gel was heated to 120 °C for 12 h to remove water. The dry residue was further heat treated at 350 °C for 2 $\sim$ 3 h to cause a reaction among them. The black precursor was sintered at 750 °C for about 12 h in air at a heating rate of 10 °C min^{-1}. As-prepared compound was found to be black in color, and the $LiMn_2O_4$ powder with intermittent grinding as such was subjected to further studies.

2.2 Characterization

The phase identification of $LiMn_2O_4$ prepared was carried out by powder X-ray diffraction (XRD, Japan) technique on a Rigaku D/Max-3 B diffractometer using Cu Kα radiation in the 15–75° range at a scan rate of 3° min^{-1} with a step width of 0.02°. The vibrational spectra of $LiMn_2O_4$ was characterized by Fourier transform infrared spectroscopy (FTIR, Tensor-27, BRUKER) using a pellet containing a mixture of KBr and the response of active material in the region of 0–1200 cm^{-1}. The surface morphologies of the synthesized compounds were obtained by means of a scanning electron microscopy (SEM, LEO 1530, Oxford Instrument).

2.3 Electrochemical experiments

For the electrochemical properties of the products, the spinel $LiMn_2O_4$ electrode used in this study was prepared by spreading a mixture comprising, by weight, 80 % $LiMn_2O_4$, 3 % acetylene black, 7 % mesocarbon microbeads, and 10 % polyvinylidene fluoride (PVdF) binder dissolved in *N*-methyl-2-pyrrolidone onto stainless foil current collector. A $LiMn_2O_4$ film electrode, a Pt wire, and a saturated calomel electrode (SCE) were used as the working, counter, and reference electrodes, respectively. An aqueous 1 M Li_2SO_4 solution was used as the electrolyte.

The cyclic voltammogram (CV) and electrochemical impedance spectroscopy (EIS) measurements were carried out at an electrochemical work station (CHI 660C). CV was obtained from the film electrode in 1 M Li_2SO_4 aqueous solution in the potential ranging from −0.20 to 1.20 V versus SCE at a scan rate of 1 mV s^{-1}. EIS was measured on the film electrode at the electrode potentials in the range of 0.12–1.2 V versus SCE by applying an ac-amplitude of 5 mV over the frequency range from 10^{-2} to 10^5 Hz, and the electrode was equilibrated for 1 h before the EIS measurements to attain steady-state conditions.

For comparison, the electrochemical measurements were also carried out in 1 M $LiPF_6$–EC:DEC:DMC (1:1:1, v/v/v) organic electrolyte by employing a three-electrode electrochemical cell in which both the reference and counter electrodes were constructed from lithium foil. In this case, all cells were assembled in a glove box filled with purified Ar gas. All the electrochemical tests were carried out at room temperature for this study.

3 Results and discussion

Figure 1 shows the FTIR absorption spectra of $LiMn_2O_4$ powders. Here the FTIR absorption of the spinel $LiMn_2O_4$ sample between 613 and 514 cm^{-1} is attributed to the asymmetric stretching modes of the MnO_6 group [24], i.e., the stretching band of O–Mn(IV)–O and Mn(III)–O. However, the Li–O stretching has not been observed, that's maybe the overlap of the Li–O and the Mn–O vibration. The XRD pattern and SEM of the as prepared $LiMn_2O_4$ are showed in Fig. 2. It can be seen that from Fig. 2a, all peaks can be indexed to the spinel structure, Fd3m space group. This structure can be described as ideally consisting of a cubic close-packed arrangement of oxygen ions at 32e sites, the Li ions occupy the tetrahedral 8a sites and the $Mn^{3+/4+}$ ions octahedral 16d sites. The scanning electron micrograph (seen in Fig. 2b) shows clearly defined octahedral shape, and their particles crystallize well with submicro-size.

Figure 3 shows the CV of spinel $LiMn_2O_4$ cathode at a scan rate of 1 mV s^{-1} in organic and aqueous electrolyte, respectively. From Fig. 3a, two anodic peaks at 4.18 and 4.05 V and two corresponding cathodic peaks at 4.06 and 3.95 V (vs. Li/Li^+) are characteristics for the $LiMn_2O_4$ cathode, corresponding the two-step reversible (de)intercalation reaction of lithium ions [25, 26]. In Fig. 3b, two pairs of redox peaks, located at 0.78/0.73 and 0.91/0.85 V (vs. SCE) are also observed, which coincide well with those in organic electrolyte and correspond to Li ion intercalation and phase transitions. It is also observed from

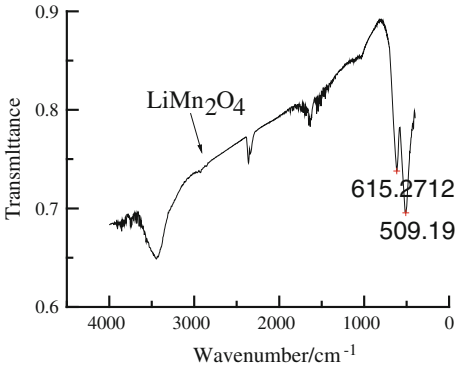

Fig. 1 FTIR spectrum of spinel $LiMn_2O_4$

Fig. 3b that it is possible to extract lithium ions from the host before the decomposition of water in neutral aqueous solution. This means that lithium intercalation/de-intercalation in spinel $LiMn_2O_4$ cathode can be viable in aqueous solution.

Figure 4 shows that the cycling performance of $LiMn_2O_4$ at 0.1 C in Li_2SO_4 aqueous solution and $LiPF_6$–EC:DEC:DMC organic electrolyte, respectively. The discharge capacities of pristine $LiMn_2O_4$ in aqueous and organic electrolyte are 57.57 and 107.16 mAh g^{-1}, and decrease to 30.92 and 85.29 mAh g^{-1} after 60 cycles, respectively. The capacity retention values of the electrode in the two electrolytes are 53.7 and 80 %, respectively. It can be seen that from Fig. 4, the capacity fading in aqueous electrolyte is more rapid in the first three cycles and then seems to become stable with the subsequent cycles. Li and Dahn [27] ascribed the severity of the capacity fading in aqueous solution to the possibility of the decomposition of water and the dissolution of lithium ion. Obviously, the spinel $LiMn_2O_4$ cathode in organic electrolyte presents more stable discharge capacity retention than that in aqueous solution.

The reason for such large difference in electrochemical performance needs further investigation. However, it can be concluded that the charge and discharge behaviors in organic electrolyte can be transferred into aqueous solution if the operating voltage is within the stable electrochemical window of water.

To further investigate the lithium ion insertion mechanism at the electrode/electrolyte interface, EIS was conducted for the $LiMn_2O_4$ cathode during the first charge cycle in different electrolytes, as presented in Figs. 5 and 6, respectively. The plots show an untypical trend for compounds of the spinel family, as could be seen from the plots in Fig. 5, a high-frequency semicircle (HFS), a semicircle in the middle-to-high frequency (MHFS) clearly emerging

Fig. 2 XRD and SEM of the as-synthesized $LiMn_2O_4$

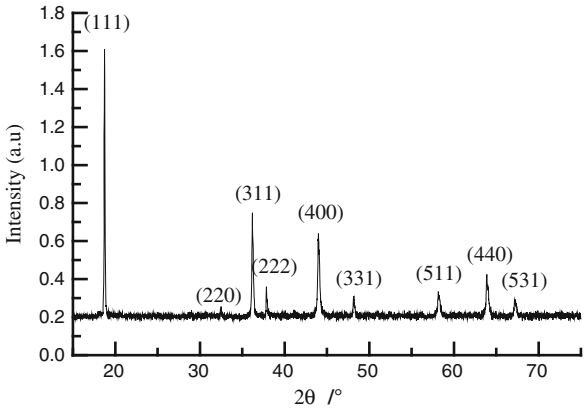

(a) XRD

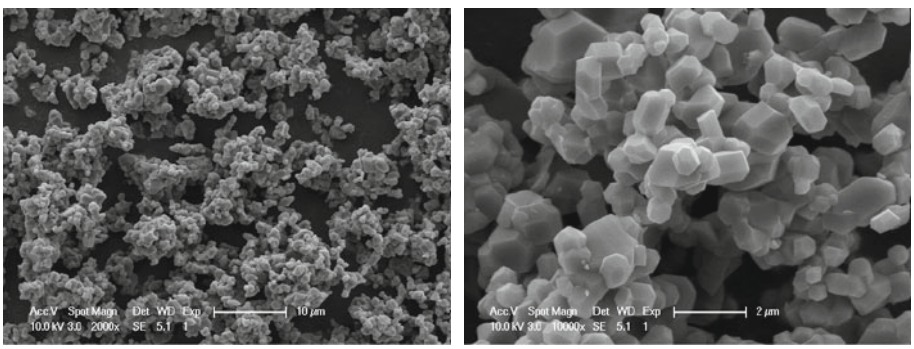

(b) SEM

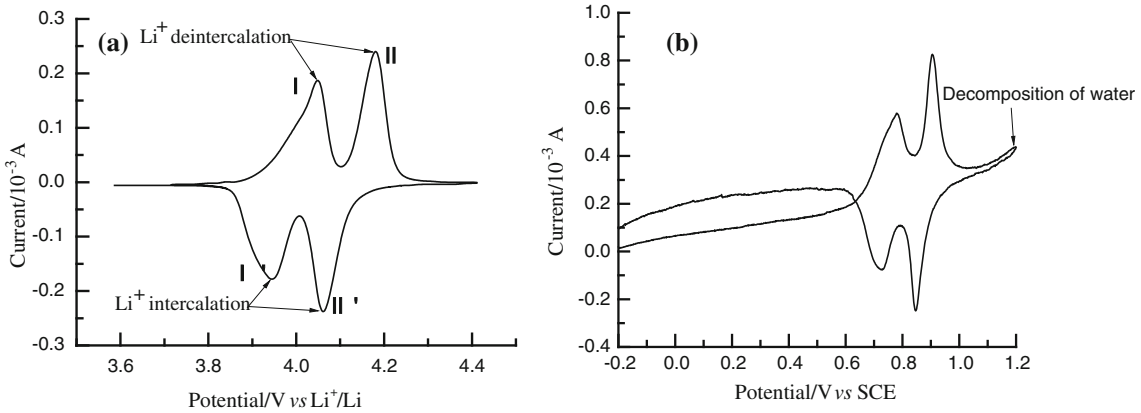

Fig. 3 Cyclic voltammetry of $LiMn_2O_4$ sample at 0.1 mV s^{-1} scan rate **a** in organic electrolyte, **b** in aqueous electrolyte

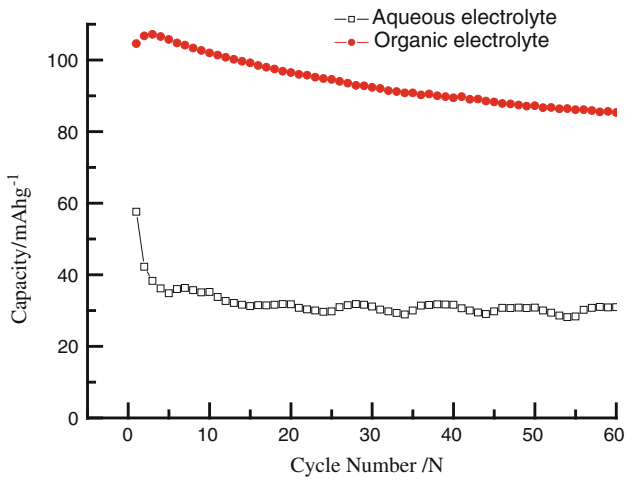

Fig. 4 The cycling performance of $LiMn_2O_4$ at 0.1 C in different electrolytes

at the potential ranging between 3.5 and 3.8 V, as well as an inclined line in the middle-to-low frequency region (LFL). With the increase of the polarization potential, the HFS and MHFS do not change so much, but the inclined line, which is strongly potential dependent, shows an increasing tendency to close on the real axis, at last forming another semicircle (middle frequency semicircle, (MFS)) and a steep sloping line in the LFL.

It is generally accepted [28–30] that in organic electrolyte the HFS is mainly caused by the passive film formation on the electrode surface from the reactions between the oxide material and the electrode solvent, and the MFS, the magnitude of which depends significantly on the electrode potential, is ascribed to the charge transfer interaction at the interface between the electrode surface film and the electrolyte. In our previous study [31], the MHFS was related to the electronic properties of the electrode material. In addition, the LFL is the Warburg impedance which is associated with a semi-infinite diffusion of lithium in the active electrode.

Comparing the EIS in aqueous electrolyte of Fig. 6 with those in organic electrolyte of Fig. 5, the impedance spectroscopy of the $LiMn_2O_4$ electrode is only composed of a semicircle and a sloping line in the whole potential range from the open circuit voltage ranging from −0.12 to 1.2 V, which is similar to Lee's results [32]. Obviously, the unique semicircle is only attributed to the charge transfer through the electrode/electrolyte interface, and the steep sloping line is assigned to solid-state diffusion of the lithium ion in the $LiMn_2O_4$ matrix. This implies that there is no lithium ion migration through the solid electrolyte interface (SEI) film, that is to say, no SEI film covered on the $LiMn_2O_4$ particles, and thus lithium ion migration stage through the interface between the electrode and aqueous electrolyte is no longer the necessary in the overall lithium intercalation process.

It is well known that the SEI film of the electrode surface can reduce the spontaneous reaction between the electrode and electrolyte, which is benefit to improve the cycling performance of electrode material. However, the bare electrode being exposed to the aqueous electrolyte would continue to be corroded by the aqueous solution in the absence of surface layer, which directly leads to the poor cycling performance of the electrode materials [1, 9, 10, 12, 16, 23]. It was reported that when $LiMn_2O_4$ material was coated by carbon material [33] or doped by divalent or trivalent ion [34], its electrochemical performance can be improved in aqueous solution.

According to experimental results obtained in this study, different equivalent circuits, as shown in Fig. 7, are proposed to fit the impedance spectra of the spinel $LiMn_2O_4$ cathode for initial charge process in organic and aqueous electrolyte. In these equivalent circuits, R_s represents the ohmic resistance in the electrolyte; R_{SEI} and R_{ct} are resistances of the SEI and the charge transfer reaction; the

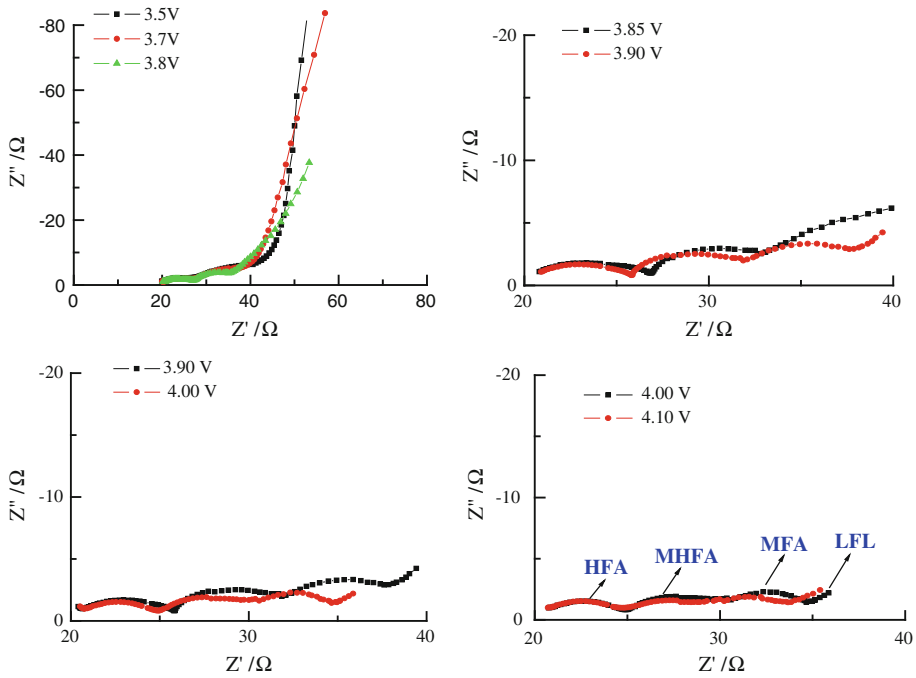

Fig. 5 EIS plots of spinel $LiMn_2O_4$ cathode in organic electrolyte for initial charge process

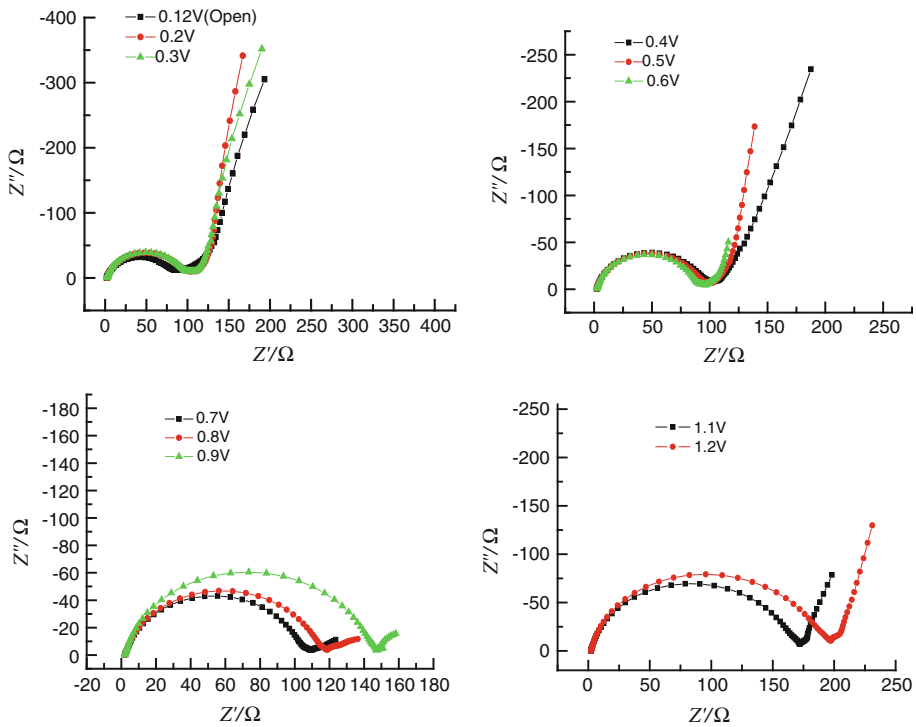

Fig. 6 EIS plots of spinel $LiMn_2O_4$ cathode in aqueous solution for initial charge process

capacitance of the SEI and the capacitance of the double layer are represented by the constant phase elements (CPE) Q_{SEI} and Q_{dl}, respectively. The LFL, however, cannot be modeled properly by a finite Warburg element; we chose therefore to replace the finite diffusion by a CPE, i.e., Q_D; The electronic resistance of the material and the associated capacitance used to characterize the electronic properties of the material are represented by R_e and the CPE Q_e, respectively. The expression for the admittance response of the CPE (Q) is

$$Y = Y_0\omega^n \cos\left(\frac{n\pi}{2}\right) + jY_0\omega^n \sin\left(\frac{n\pi}{2}\right), \quad (1)$$

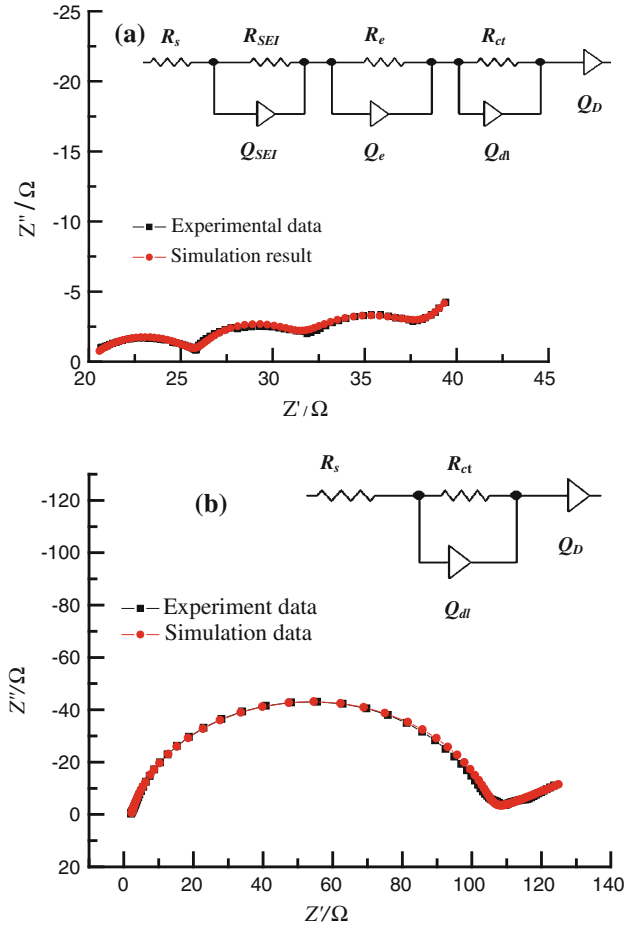

Fig. 7 Comparison of EIS experimental data in the first charge process with simulation results using different equivalent circuits **a** in organic electrolyte at 3.9 V (vs. Li/Li^+) and **b** in aqueous solution at 0.6 V (vs. SCE)

where ω is the angular frequency, j is the imaginary unit, and Y_0 is the admittance constant and independent of frequency. A CPE represents a resistor when $n = 0$, a capacitor with capacitance of C when $n = 1$, an inductor when $n = -1$, and a Warburg resistance when $n = 0.5$.

Figure 7 shows the simulated impedance spectra compared with experimental EIS data in initial charge process in organic electrolyte at 3.9 V (vs. Li/Li^+) and in aqueous solution at 0.6 V (vs. SCE). Equivalent circuit parameters obtained from fitting the experimental impedance spectra from Figs. 5 and 6 are accordingly listed in Tables 1 and 2, and the relative standard deviations for almost all parameters, obtained from fitting the experimental impedance spectra, do not exceed 15 %. It is seen that both the proposed models can describe the experimental data satisfactorily.

On comparison of Tables 1 and 2, we find that the value of ohmic resistance (R_s) of aqueous solution (19.96 Ω) is greater than that of organic electrolyte (2.05 Ω), which may be attributed to the higher ionic conductivity of aqueous electrolyte [3, 6]. However, the value of charge transfer resistance (R_{ct}) in aqueous solution is much higher than that of organic electrolyte, which may be caused by the uneven compaction or the nonuniform thickness of electrode film.

The parameters of the equivalent circuit from fitting the experimental impedance data of the $LiMn_2O_4$ electrode with the increase of the potential in aqueous solution are shown in Fig. 8. The R_{ct} versus E plot is supposed to behave according to the following classical equation [35]:

$$R_{ct} = 1/fFk_0Ac_O^{0.5}c_R^{0.5} \quad (2)$$

In this equation, f denotes the usual electrochemical constant (equal to F/RT with F and R, denoting Faraday and gas constant, respectively; T, is the absolute temperature); and k_0 is the heterogeneous rate constant, respectively. It should be remembered that using Eq. (2) the total concentration of available intercalation sites, c_T, is constant, i.e., $c_O + c_R = c_T$. The concentration of the red-form, c_R, and that of the ox-form, c_O, are identified by means of the concentration of lithium ions and unoccupied intercalation sites, respectively. Eq. (2) predicts clearly a rapid increase in R_{ct} as $c_O \to c_T$ or $c_R \to c_T$, i.e., in either completely intercalated or de-intercalated state. It is observed from Fig. 8a that R_{ct} is high at the low and high potentials and minimal at middle potentials in the charge process. The results confirm that Eq. (2) can be used to interpret properly the experimental data, and thus the unique semicircle in the high frequency is undoubtedly attributed to the charge transfer process.

In Fig. 8b, the variation of Q_{dl}–Y_0 exhibits a similar behavior as that of the R_{ct} in the charge process. This implies that the double layer capacitance on the spinel $LiMn_2O_4$ electrode surface in aqueous electrolyte is mainly affected by lithium ion insertion/extraction, i.e., the process of lithium ion insertion/extraction is easier, the double layer capacitance value is smaller. However, the Q_{dl}–n increases overall with the increase of the polarization potential in Fig. 8c, confirming the decrease of the porosity of the composite electrode and roughness of the electrode surface.

4 The physical mechanism of lithium insertion and de-insertion in aqueous solution

In the past, several models [28, 36, 37] have been proposed to explain the impedance response of the insertion materials of lithium ion batteries in organic electrolyte, including graphite anode and cathode materials such as $LiMn_2O_4$, $LiNiO_2$, $LiCoO_2$, and so on. One of the most convincing models was Barsoukov's [36, 37], because the electron conduction and change of the particle structure or new phase

Table 1 Equivalent circuit parameters obtained from fitting the experimental impedance spectra at 3.9 V (vs. Li/Li^+) in the first charge process for spinel $LiMn_2O_4$ in $LiPF_6$–EC:DEC:DMC organic electrolyte

Parameters	Valves	Uncertainty (%)
R_s	19.96	0.31
R_{SEI}	6.08	1.88
$Q_{SEI}-Y_0$	2.46×10^{-4}	11.14
$Q_{SEI}-n$	0.65	1.92
R_e	5.59	3.85
Q_e-Y_0	6.63×10^{-3}	6.05
Q_e-n	0.88	2.14
R_{ct}	6.04	9.82
$Q_{dl}-Y_0$	0.15	7.51
$Q_{dl}-n$	0.88	4.18
Q_D-Y_0	1.54	23.91
Q_D-n	0.70	9.06

Table 2 Equivalent circuit parameters obtained from fitting the experimental impedance spectra at 0.6 V (vs. SCE) in the first charge process for spinel $LiMn_2O_4$ in Li_2SO_4 aqueous solution

Parameters	Valves	Uncertainty (%)
R_s	2.05	2.65
$Q_{dl}-Y_0$	1.60×10^{-5}	3.21
$Q_{dl}-n$	0.89	0.46
R_{ct}	101.70	0.70
Q_D-Y_0	0.10	8.03
Q_D-n	0.32	6.67

formation in electrode materials were taken into account by them. They supposed that electrochemical kinetics characteristic for battery materials in organic electrolyte was represented during lithium ion insertion by several common steps: (i) ionic charge conduction through electrolyte in pores of active layer and electronic charge conduction through conductive part of active layer, (ii) Li ions diffusion through surface insulating layer of active material, (iii) electrochemical reaction on the interface of active material particles including electron transfer, (iv) Li ions diffusion in the solid phase, and (v) a capacitive behavior that is related to the occupation of lithium ions and phase-transfer if several phases are present. Among these steps of lithium ion insertion, the ionic charge conduction through electrolyte in pores of active layer (i) usually gives no semicircle in the frequency range $10^5 \sim 10^{-2}$ Hz range because of their high characteristic frequencies. The two processes (ii) and (iii) give their own semicircles at each characteristic frequency, respectively, and these components of resistance appear as a Z' intercept in the Nyquist plot. The process of Li ions diffusion in the solid phase (iv) gives the Warburg impedance, which is observed as a straight line with an angle of 45° from the Z' axis. The capacitive behavior that is related to the occupation of lithium ions and phase-transfer would give straight line perpendicular to Z' axis and a semicircle in the Nyquist plot (commonly below 10^{-2} Hz), respectively. However, most active material is electronic semiconductor and so an electronically conductive material such as carbon black is essential, and the importance of electron conduction in electrode materials was obviously underestimated by Barsoukov et al., and so they always could not get three semicircles in their research; their results commonly consisted of three parts, namely, a semicircle in high frequency region, another semicircle in middle frequency region, a Warburg-type element in LFL at intermediate intercalation degrees, but without the MHFS. In our previous study [31], a modified model was put forward based on the experimental results, and the EIS spectra in the frequency range $10^5 \sim 10^{-2}$ Hz were interpreted in terms of the following physical phenomena in an order of decreasing frequency: (i) a HFS because of the presence of SEI film, (ii) a middle to HFS related to the electronic properties of the material, (iii) a MFS associated with charge transfer through the electrode/electrolyte interface, and finally, (iv) the very low-frequency incline line attributed to the solid-state diffusion of lithium ion in the active matrix.

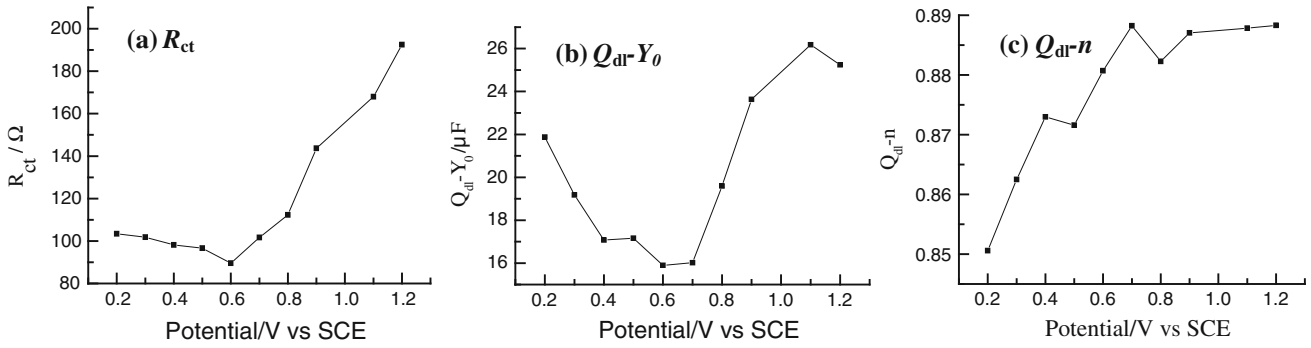

Fig. 8 Variation of R_{ct} (**a**), $Q_{dl}-Y_0$ (**b**), and $Q_{dl}-n$ (**c**) with the potential of spinel $LiMn_2O_4$ in aqueous solution in initial charge process

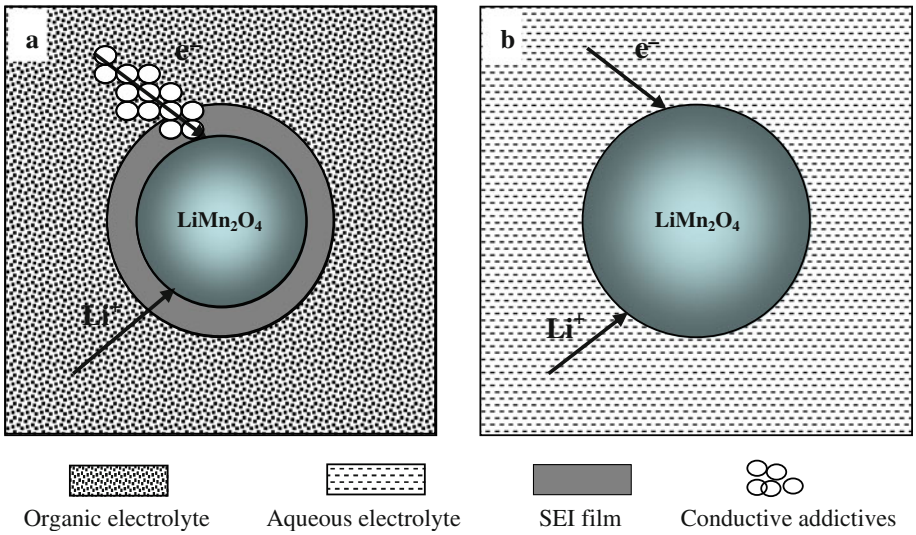

Fig. 9 Pictorial representation models for lithium ion insertion/de-insertion into the intercalation electrode in **a** organic electrolyte and **b** aqueous electrolyte

So far, the modified models [31] do provide the excellent interpretation of insertion/de-insertion reaction mechanism in organic electrolyte; however, the insertion/de-insertion reaction mechanisms in aqueous solution have changed, because of the lack of SEI film at the electrode/electrolyte interface and the high ionic conductivity of aqueous solution. Obviously, lithium ion insertion of spinel $LiMn_2O_4$ in aqueous electrolyte consists of the following four steps: (i) Li ion transfer in aqueous solution; (ii) Li ion diffusion from the aqueous solution to the electrode surface; (iii) Charge transfer; and (iv) Li ion diffusion in the solid phase of the spinel matrix.

For comparison, Fig. 9 gives pictorial representation model for lithium ion insertion/de-insertion into the intercalation electrode in organic and aqueous electrolytes, respectively. In Fig. 9a, Li ions from the organic electrolyte first pass through the SEI film and then reach the $LiMn_2O_4$ surface, and at same time, equivalent electrons are transferred to the $LiMn_2O_4$ surface. It is well known that the SEI film is ionically conducting but electronically insulating [38]. If the conductive addictives dispersing in the active material is coated by the SEI film, then the electron charge conduction proceeds by way of the electronic tunneling effect. Otherwise, the electron transports directly to the points where the active material and the conductive material meet, and then the electron diffuses inside active particles. However, in aqueous solution (in Fig. 9b), Li ions migrate to the $LiMn_2O_4$ surface directly from the aqueous electrolyte, and simultaneously, the electrons are easily captured from the aqueous electrolyte, or the active material and the conductive material meet and then diffuse inside active particles. Obviously, the above reaction process occurs easily because of the high conductivity of aqueous electrolyte and the fast charge transfer kinetics without the impeding effect of the surface layer in aqueous electrolyte.

5 Conclusions

Measurements of cyclic voltammetry and EIS of $LiMn_2O_4$ in 1 M Li_2SO_4 aqueous solution show that the intercalation and de-intercalation of lithium ions are similar to those in organic electrolytes, but the lithium ion insertion mechanism at the electrode/electrolyte interface is different. There are two steps of lithium ion intercalation/de-intercalation in aqueous solution, with locations at $E_{SCE} = 0.78/0.73$ V, 0.91/0.85 V, which agree well with those in organic electrolyte at $E_{Li/Li^+} = 4.05/3.95$ and 4.06/4.18 V. The discharge capacity values of pristine $LiMn_2O_4$ in aqueous and organic electrolytes are 57.57 and 107.16 mAh g^{-1}, and the capacity retention values of the electrode are 53.7 and 80 % after 60 cycles, respectively. The Nyquist plots for spinel $LiMn_2O_4$ cathode in aqueous solution show only one semicircle, which corresponds to the charge transfer reaction, unlike the three semicircles obtained in organic electrolyte. There is no SEI formation on the surface of spinel $LiMn_2O_4$ electrode in aqueous electrolyte. The charge transfer reaction resistance first decreases and then increases gradually with the increase of the potential, and a suitable model is proposed to explain the impedance response of the insertion materials of lithium ion batteries in aqueous solution.

Acknowledgments The project was supported by the Fundamental Research Funds for the Central Universities (2010LKHX03,

2010QNB04, and 2010QNB05) and funded by the Priority Academic Program Development of Jiangsu Higher Education Institutions.

References

1. Broussely M, Planchat JP, Rigobert G, Virey D, Sarre G (1997) J Power Sources 68:8
2. Li W, Dahn JR, Wainwright DS (1994) Science 264:1115
3. Joachim K, Chaussee R, Hiroshi M, Hisakazu U, Hitoshi I, Motoyuki T (2000) Electrochim Acta 46:59
4. Wang YG, Xia YY (2005) Electrochem Commun 7:1138
5. Wang GX, Zhong S, Bradhurst DH, Dou SX, Liu HK (1998) J Power Sources 74:198
6. Li N, Patrissi CJ, Che G, Martin CR (2000) J Electrochem Soc 147:2044
7. Ruffo R, Wessells C, Robert HA, Cui Y (2009) Electrochem Commun 11:247
8. Xia YY, Luo JY, Wang YG (2008) Chinese J Power Sources 32:431
9. Wang GJ, Yang LC, Qu QT, Wang B, Wu YP, Holze R (2010) J Solid State Electrochem 14:865
10. Zeng XL, Huang YY, Luo FL, He YB, Tong DG (2010) J Sol Gel Sci Techn 54:1
11. Ruffo R, Mantia FL, Wessells C, Huggins RA, Cui Y (2011) Solid State Ionics 192:289
12. Wang GJ, Qu QT, Wang B, Shi Y, Tian S, Wu YP, Holze R (2009) J Power Sources 189:503
13. Wang GJ, Zhao NH, Yang LC, Wu YP, Wu HQ, Holze R (2007) Electrochim Acta 52:4911
14. Wang GJ, Fu LJ, Zhao NH, Yang LC, Wu YP, Wu HQ (2007) Angew Chem Int Ed 46:295
15. Wang GJ, Zhang HP, Fu LJ, Wang B, Wu YP (2007) Electrochem Commun 9:1873
16. Wang HB, Huang KL, Zeng YQ, Yang S, Chen LQ (2007) Electrochim Acta 52:3280
17. Liu XH, Saito T, Doi T, Okada S, Yamaki J (2009) J Power Sources 189:706
18. Wessells C, Huggins RA, Cui Y (2011) J Power Sources 196:2884
19. Zhao MS, Zheng QY, Wang F, Dai WM, Song XP (2011) Electrochim Acta 56:3781
20. Wang HB, Zeng YQ, Huang KL, Liu SQ, Chen LQ (2007) Electrochim Acta 52:5102
21. Minakshi M, Singha P, Appadoo D, Martin DE (2011) Electrochim Acta 56:43
22. Wu MS, Wang MJ, Jow JJ, Yang WD, Hsieh CY, Tsai HM (2008) J Power Sources 185:1420
23. He P, Liu JL, Cui WJ, Luo JY, Xia YY (2011) Electrochim Acta 56:2351
24. Wu C, Wang ZX, Wu F, Chen LQ, Huang XJ (2001) Solid State Ionics 144:277
25. Sigala C, La Salle AL, Piffard Y, Guyomard D (2001) J Electrochem Soc 148:A819
26. Kamarulzaman N, Yusoff R, Kamarudin N, Shaari NH, Abdul Aziz NA, Bustam MA, Blagojevic N, Elcombe M, Blackford M, Avdeev M, Arof AK (2009) J Power Sources 188:274
27. Li W, Dahn JR (1995) J Electrochem Soc 142:1742
28. Aurbach D, Levi MD, Levi E, Telier H, Markovsky B, Salitra G, Heider U, Hekier L (1998) J Electrochem Soc 145:3024
29. Aurbach D, Gamolsky K, Markovsky B, Salitra G, Gofer Y, Heider U, Oesten R, Schmidt M (2000) J Electrochem Soc 147:1322
30. Aurbach D, Levi MD, Gamulski K, Markovsky B, Salitra G, Levi E, Heider U, Heider L, Oesten R (1999) J Power Source 81–82:472
31. Zhuang QC, Wei T, Du LL, Cui YL, Fang L, Sun SG (2010) J Phys Chem C 114:8614
32. Lee JW, Pyun S (2004) Electrochim Acta 49:753
33. Chen SY, Mi CH, Su LH, Gao B, Fu QB, Zhang XG (2009) J Appl Electrochem 39:1943
34. Zhao MS, Zhang B, Huang GL, Dai WM, Wang F, Song XP (2012) Energy Fuels 26:214
35. Levi MD, Gamolsky K, Aurbach D, Heide U, Oesten R (2000) On electrochemical impedance measurements of LixCo0.2Ni0.8O2 and LixNiO2 intercalation electrodes. Electrochimica Acta 45:1781–1789
36. Barsoukov E, Kim DH, Lee HS, Lee H, Yakovleva M, Gao Y, Engel JF (2003) Solid State Ionics 161:19
37. Barsoukov E, Kim JH, Yoon CO, Lee H (1999) Solid State Ionics 116:249
38. Hjelm AK, Lindbergh G (2002) Electrochim Acta 47:1747